Contribution from the Department of Chemistry, University of Florence, Via Gino Capponi 7, 50121 Florence, Italy, and Institute of Agricultural Chemistry, University of Bologna, Viale Berti Pichat 10, 40127 Bologna, Italy

^{1}H NMR Spectra of Oxidized High-Potential Iron–Sulfur Protein (HiPIP) from *Rhodocyclus gelatinosus*. A Model for Oxidized HiPIPs

Lucia Banci,[†] Ivano Bertini,*[,†] Fabrizio Briganti,[†] Claudio Luchinat,[‡] Andrea Scozzafava,[†] and Margarita Vicens Oliver[†]

Received April 9, 1991

The assignment of the β-CH_2 cysteinyl resonances of the oxidized and reduced high-potential iron protein (HiPIP) from *Rhodocyclus gelatinosus* (formerly *Rhodopseudomonas gelatinosa*) has been proposed through ^{1}H NOE, NOESY, and EXSY measurements. The interest has been focused on the oxidized protein for which the comparison of the isotropic shift values and their temperature dependence with those of *Chromatium vinosum* and *Ectothiorhodospira halophila* II HiPIPs is rationalized on the basis of theoretical calculations. Such calculations have been performed by utilizing a magnetic exchange spin Hamiltonian with and without the introduction of a double-exchange parameter. No appreciable difference in the energy level pattern is noticed between the two treatments. All the data point toward a cluster with a mixed-valence pair Fe(III)–Fe(II) and two pure Fe(III) ions. The inequivalence between the two Fe(III) ions distinguishes the three proteins. The low-temperature Mössbauer spectra of *C. vinosum* are rationalized.

Introduction

$[Fe_4S_4]^{n+}$ clusters have attracted for a long time the interest of inorganic chemists from the synthetic and structural points of view[1-3] and, more recently, also for the theoretical aspects relative to the understanding of the electron delocalization in such systems.[4-10]

In naturally occurring proteins, these clusters are used to perform one-electron transfer.[11-15] The tuning of the electronic properties of the cluster by the protein is such that either the $[Fe_4S_4]^{3+}/[Fe_4S_4]^{2+}$ or the $[Fe_4S_4]^{2+}/[Fe_4S_4]^{+}$ pairs are stabilized. One goal in the investigation of such proteins is that of understanding the oxidation states of the single metal ions and the electronic delocalization within the cluster.

^{1}H NMR spectra of iron–sulfur proteins have been reported in the literature.[16-24] The β-CH_2 protons of cysteines bound to the cluster experience large contact shifts, which are ultimately determined by the amount of unpaired electrons present over the iron atom at which the cysteine is bound.[16,25] We have already shown, by studying the oxidized form of high-potential iron–sulfur proteins (HiPIP hereafter) extracted from *Chromatium vinosum*[26] and from *Ectothiorhodospira halophila*,[27] that eight signals spread between +110 and −40 ppm can be assigned to the eight protons of the four β-CH_2 cysteine ligands. The chemical shifts and the temperature dependence of these signals represent experimental parameters that can be used for testing the validity of theoretical models.

In the oxidized protein from *E. halophila* ($3Fe^{3+}$–$1Fe^{2+}$) four β-CH_2 protons are shifted upfield and other four shifted downfield.[27] With some assumptions based on the Mössbauer data on the analogous protein from *C. vinosum*[28] the upfield signals have been assigned to β-CH_2 protons of the cysteines coordinated to two iron(III) ions, whereas the four downfield shifted signals would arise from the β-CH_2 protons of the cysteines coordinated to the other two iron ions (one iron(III) and one iron(II)), which would constitute the mixed-valence pair.[26,27] In *C. vinosum* the experimental spectrum shows only two signals upfield, whereas six are downfield; of the latter six, the two nearest to the diamagnetic region have an anti-Curie temperature dependence, opposite to that of the other downfield signals.[26] Despite the differences with the spectra of the oxidized protein from *E. halophila*, again a simplified model was proposed with two iron(III) ions and one mixed-valence pair.[26] In this case, the four β-CH_2 protons of the cysteines coordinated to the two iron(III) ions have been assigned to the two upfield signals and to the two downfield signals experiencing anti-Curie temperature dependence.[26] The mixed-valence-pair description of the other four downfield signals again derives from the Mössbauer data on the *C. vinosum* protein, which are consistent with two iron ions at oxidation number equal to +2.5.[28]

In order to better understand the above patterns of the shifts and to relate them to the electronic structure of the cluster, we have studied the HiPIP from *Rhodocyclus gelatinosus* (formerly classified as *Rhodopseudomonas gelatinosa*). Furthermore, we

[†] University of Florence.
[‡] University of Bologna.

(1) Holm, R. H.; Ciurli, S.; Weigel, J. A. *Prog. Inorg. Chem.* **1990**, *38*, 1.
(2) Berg, J. M.; Holm, R. H. In *Iron-Sulfur Proteins*; Spiro, T. G., Ed.; Wiley-Interscience: New York, 1982; Vol. 4, p 1.
(3) Hagen, K. S.; Reynolds, J. G.; Holm, R. H. *J. Am. Chem. Soc.* **1981**, *103*, 4054.
(4) Noodleman, L. *Inorg. Chem.* **1988**, *27*, 3677.
(5) Münck, E.; Papaefthymiou, V.; Surerus, K. K.; Girerd, J. J. In *Metals in Proteins*; ACS Symposium Series; Que, L., Ed.; American Chemical Society: Washington, DC, 1988; and references therein.
(6) Papaefthymiou, V.; Girerd, J.-J.; Moura, I.; Moura, J. J. G.; Munck, E. *J. Am. Chem. Soc.* **1987**, *109*, 4703.
(7) Girerd, J.-J. *J. Chem. Phys.* **1983**, *79*, 1776.
(8) Borsch, S. A.; Chibotaru, L. F. **1989**, *135*, 375.
(9) Noodleman, L. *Inorg. Chem.* **1991**, *30*, 246.
(10) Blondin, G.; Girerd, J. J. *Chem. Rev.* **1990**, *90*, 1359.
(11) Carter, C. W.; Kraut, J.; Freer, S. T.; Alden, R. A.; Sieker, L. C.; Adman, E.; Jensen, L. H. *Proc. Natl. Acad. Sci. U.S.A.* **1972**, *69*, 3526.
(12) Carter, C. W.; Kraut, J.; Freer, S. T.; Alden, R. A. *J. Biol. Chem.* **1974**, *249*, 6339.
(13) Aldman, E. T.; Sieker, L. C.; Jensen, L. H. *J. Biol. Chem.* **1974**, *248*, 3987.
(14) Fukuyama, K.; Nagahara, Y.; Tsikihara, T.; Katsube, Y.; Hase, T.; Matsubara, H. *J. Mol. Biol.* **1988**, *199*, 183.
(15) Stout, C. D. In *Iron-Sulfur Proteins*; Spiro, T. G., Ed.; Wiley-Interscience: New York, 1982; Chapter 3.
(16) Phillips, W. D. In *NMR of Paramagnetic Molecules, Principles and Applications*; La Mar, G. N., Horrocks, W. DeW., Jr., Holm, R. H., Eds.; Academic Press: New York, 1973; Chapter 11. Phillips, W. D.; Poe, M. In *Iron-Sulfur Proteins*; Lovenberg, W., Ed.; Academic Press: New York, 1977; Vol. 3, Chapter 7.
(17) Bertini, I.; Briganti, F.; Luchinat, C.; Scozzafava, A. *Inorg. Chem.* **1990**, *29*, 1874.
(18) Gaillard, J.; Moulis, J.-M.; Meyer, J. *Inorg. Chem.* **1987**, *26*, 320.
(19) Nettesheim, D. G.; Meyer, J. L.; Feinberg, B. A.; Otvos, J. D. *J. Biol. Chem.* **1983**, *258*, 8235.
(20) Krishnamoorthi, R.; Markley, J. L.; Cusanovich, M. A.; Prysiecki, C. T.; Meyer, T. E. *Biochemistry* **1986**, *25*, 60.
(21) Krishnamoorthi, R.; Cusanovich, M. A.; Meyer, T. E.; Prysiecki, C. T. *Eur. J. Biochem.* **1989**, *181*, 81.
(22) Sola, M.; Cowan, J. A.; Gray, H. B. *Biochemistry* **1989**, *28*, 5261–5268.
(23) Cowan, J. A.; Sola, M. *Biochemistry* **1990**, *29*, 5633.
(24) Bertini, I.; Luchinat, C. *NMR of Paramagnetic Molecules in Biological Systems*; Benjamin/Cummings: Menlo Park, CA, 1986.
(25) *NMR of Paramagnetic Molecules, Principles and Applications*; La Mar, G. N., Horrocks, W. DeW., Jr., Holm, R. H., Eds.; Academic Press: New York, 1973.
(26) Bertini, I.; Briganti, F.; Luchinat, C.; Scozzafava, A.; Sola, M. *J. Am. Chem. Soc.* **1991**, *113*, 1237–1245.
(27) Banci, L.; Bertini, I.; Briganti, F.; Luchinat, C.; Scozzafava, A.; Vicens Oliver, M. *Inorg. Chim. Acta*, in press.
(28) Middleton, P.; Dickson, D. P. E.; Johnson, C. E.; Rush, J. D. *Eur. J. Biochem.* **1980**, *104*, 289.

0020-1669/91/1330-4517$02.50/0

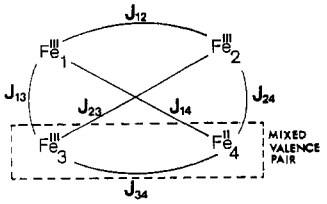

Figure 1. Heisenberg exchange-coupling scheme in the $[Fe_4S_4]^{3+}$ cluster of oxidized HiPIPs. The extra electron is arbitrarily placed on Fe_4 in the absence of delocalization and on the Fe_3Fe_4 pair in the presence of two-center delocalization.

have extended the calculations[26] in order to be able to predict the shift patterns when the two iron(III) ions become inequivalent. We present here a model that is consistent with the observed patterns of the hyperfine shifts for the HiPIPs from *E. halophila*, *C. vinosum*, and *R. gelatinosus* with temperature and provides information on the electronic structure of the metal clusters.

Experimental Section

Materials and Methods. All chemicals used throughout were of the best quality available. *R. gelatinosus* HiPIP was prepared and purified as previously reported.[29] Experiments in 99.8% D_2O, 30 mM NaH_2PO_4 were performed by solvent exchange utilizing an ultrafiltration Amicon cell equipped with a YM5 membrane; at least five changes of deuterated buffer were performed to ensure satisfactory solvent exchange. The protein samples (2–6 mM) were reduced or oxidized by addition of small amounts of 0.1 M sodium dithionite or potassium hexacyanoferrate(III), respectively; the extent of reduction/oxidation was monitored by measuring the area of the NMR peaks corresponding to the different redox species. The pH values are reported as uncorrected pH-meter readings (pH*).

Spectroscopic Measurements. ^1H NMR measurements were carried out on a Bruker AMX 600 spectrometer operating at 600.13 MHz. Typically 1000–5000 transients were acquired by utilizing the Super-WEFT (D–180–τ–90–AQ) pulse sequence.[30]

T_1 measurements were performed by utilizing the inversion recovery sequence.[31] The transmitter frequencies were placed at various values over the spectrum in such a way to properly excite the various groups of signals.

^1H NOE and saturation-transfer measurements were performed by collecting 8–16K data points over 50–125-kHz band widths. The water signal was suppressed with the Super-WEFT pulse sequence with recycle times (AQ + D) of 40–90 ms and τ values of 35–80 ms. The resonances under investigation were saturated by utilizing a selective CW saturation during the time τ. Difference spectra were collected directly by applying the decoupler frequency, alternatively, at frequencies ω, $\omega + \delta$, ω, and $\omega - \delta$, where ω is the frequency of the irradiated signal and δ is an offset typically of the order of the signal line width. The receiver phase was properly alternated in such a way that the scans with the decoupler frequency on-resonance were added and those with the decoupler frequency off-resonance subtracted. This sequence scheme allows the obtainment of good difference spectra minimizing hardware instabilities. Each experiment, run in block-averaging mode, consisted usually of 2–10 blocks of 16 384 scans each. Exponential multiplication of the free induction decay improved the signal-to-noise ratio, introducing 5–15-Hz additional line broadening.

2D NMR NOESY and EXSY spectra[32,33] on 60-kHz spectral width were acquired with the standard NOESY pulse sequence D–90–t_1–90–t_m–90–t_2 (AQ). EXSY and NOESY experiments were recorded with 1K data points in t_2 and 512 t_1 values with 4K scans per FID. In the EXSY experiment reported D = 130 ms, t_m = 5 ms, and t_2 = 8 ms, and in the NOESY experiment D = 105 ms, t_m = 10 ms, and t_2 = 4 ms. Prior to Fourier transformation the 2D data matrix was multiplied by a $\pi/2$-shifted sine-squared function in both t_1 and t_2 and zero-filled in t_1 to 1K. NOE and saturation-transfer analyses were performed as previously reported.[26,33,34]

Theoretical Calculations. The scheme of the Heisenberg exchange coupling in $[Fe_4S_4]^{3+}$ clusters of oxidized HiPIPs is shown in Figure 1. Heisenberg exchange coupling within the four-iron cluster generates a set of different energy levels characterized by total S_i values. The eigenvalues and eigenfunctions can be obtained analytically or numerically according to the symmetry of the Heisenberg coupling scheme (see Appendix). The contact shift contribution, originating from each total S_i level of the cluster, is given by

$$\left[\frac{\Delta\nu}{\nu_0}\right]_i = -\frac{1}{\hbar\gamma_N B_0} A_i' \langle \hat{S}_z \rangle_i \tag{1}$$

where B_0 is the external magnetic field, γ_N is the nuclear magnetogyric ratio, A_i' is the contact hyperfine constant between the resonating nucleus and each S_i level, and $\langle \hat{S}_z \rangle_i$ is the expectation value of the total spin operator $\hat{S}_z$. When the Boltzmann population is taken into consideration, the overall contact shift can be evaluated as

$$\frac{\Delta\nu}{\nu_0} = -\frac{1}{\hbar\gamma_N B_0} \sum_i A_i' \langle \hat{S}_z \rangle_i \frac{(2S_i + 1)e^{-E_i/kT}}{\sum_i (2S_i + 1)e^{-E_i/kT}} \tag{2}$$

where E_i represents the energy of the ith coupled level.

By focusing on the contribution of only one metal ion, m, to the contact hyperfine shift of the nucleus, we can relate A_i' of eqs 1 and 2 with A_m for the same uncoupled metal ion m

$$A_i'/A_m = \langle \hat{S}_{mz} \rangle_i / \langle \hat{S}_z \rangle_i = C_{im} \tag{3}$$

and therefore

$$A_i' = A_m C_{im} \tag{4}$$

where A_m is the hyperfine coupling constant between the resonating nucleus and the metal ion m when alone, i.e. not included in a magnetically coupled system.

$\langle \hat{S}_{mz} \rangle_i$ of a given metal ion m in the cluster is calculated by operating with $\hat{S}_z$ on the S_m spin wave function contributing to a given S_i. Therefore, if A_m can be estimated from monometallic complexes, A_i' can be calculated through eq 1 and the shift, due to a metal center, predicted by inserting the values of A_i' and $\langle \hat{S}_z \rangle_i$ in eq 2:

$$\frac{\Delta\nu}{\nu_0} = \frac{g_e\mu_B}{\hbar\gamma_1 3kT} A_m \frac{\sum_i C_{im} S_i(S_i + 1)(2S_i + 1)e^{-E_i/kT}}{\sum_i (2S_i + 1)e^{-E_i/kT}} \tag{5}$$

A_m is taken equal for all protons, the difference between geminal protons being ascribed at a first approximation to the dihedral angle between the Fe–S–C and S–C–H planes. In the present calculations A_m is always taken equal to 1 MHz, which is in agreement with the experimental data for monomeric systems.[37]

For Hamiltonian (A2) (see Appendix) the C_{im} coefficients for each level i are given by[4,26]

$$C_{im} = \alpha_m \gamma_m / \Delta_m \tag{6}$$

where

$$\alpha_m = \{\beta_1[S_{mn}(S_{mn} + 1) + S_m(S_m + 1) - S_n(S_n + 1)] + \beta_2[S_{mn}(S_{mn} + 1) - S_m(S_m + 1) + S_n(S_n + 1)]\}/2$$

$$\gamma_m = [S(S + 1) + S_{mn}(S_{mn} + 1) - S_{kl}(S_{kl} + 1)]/2$$

$$\Delta_m = S_{mn}(S_{mn} + 1)S(S + 1)$$

and m and n correspond to the iron sites of one pair (1–2 or 3–4) whereas k and l correspond to the iron sites of the other pair. Furthermore, $\beta_1 = \beta_2 = {}^1/_2$ in the presence of delocalization whereas $\beta_1 = 1$ and $\beta_2 = 0$ in the absence of delocalization within the mn iron site pair. The analytical solution for Hamiltonian (A4) (see Appendix) gives

$$C_{i1} = \alpha_+\beta_- \qquad C_{i2} = \alpha_- \qquad C_{i3} = \alpha_+\beta_+\gamma_+ \qquad C_{i4} = \alpha_+\beta_+\gamma_- \tag{7}$$

where

$$\alpha_\pm = {}^1/_2 \pm [S_{341}(S_{341} + 1) - S_2(S_2 + 1)]/[2S(S + 1)]$$

$$\beta_\pm = {}^1/_2 \pm [S_{34}(S_{34} + 1) - S_1(S_1 + 1)]/[2S_{341}(S_{341} + 1)]$$

$$\gamma_\pm = {}^1/_2 \pm [S_3(S_3 + 1) - S_4(S_4 + 1)]/[2S_{34}(S_{34} + 1)]$$

(29) Bartsch, R. G. *Methods Enzymol.* **1978**, *53*, 329.
(30) Inubushi, T.; Becker, E. D. *J. Magn. Reson.* **1983**, *51*, 128.
(31) Vold, R. L.; Waugh, J. S.; Klein, M. P.; Phelps, D. E. *J. Chem. Phys.* **1968**, *48*, 3831.
(32) Bodenhausen, G.; Ernst, R. R. *J. Am. Chem. Soc.* **1982**, *104*, 1304.
(33) Ernst, R. R. Bodenhausen, G.; Wokaun, A. *Principles of Nuclear Magnetic Resonance in One and Two Dimensions*; Clarendon Press: Oxford, England, 1987; p 490. Jenkins, B. J.; Lauffer, R. B. *Inorg. Chem.* **1988**, *27*, 4730.
(34) Noggle, J. H.; Shirmer, R. E. *The Nuclear Overhauser Effect*; Academic: New York, 1971. Neuhaus, D.; Williamson, M. *The Nuclear Overhauser Effect in Structural and Conformational Analysis*; VCH Publ.: New York, 1989.
(35) Barbaro, P.; Bencini, A.; Bertini, I.; Briganti, F.; Midollini, S. *J. Am. Chem. Soc.* **1990**, *112*, 7238.
(36) Bertini, I.; Briganti, F.; Luchinat, C. *Inorg. Chim. Acta* **1990**, *175*, 9.
(37) Banci, L.; Bertini, I.; Luchinat, C. *Struct. Bonding* **1990**, *72*, 113.

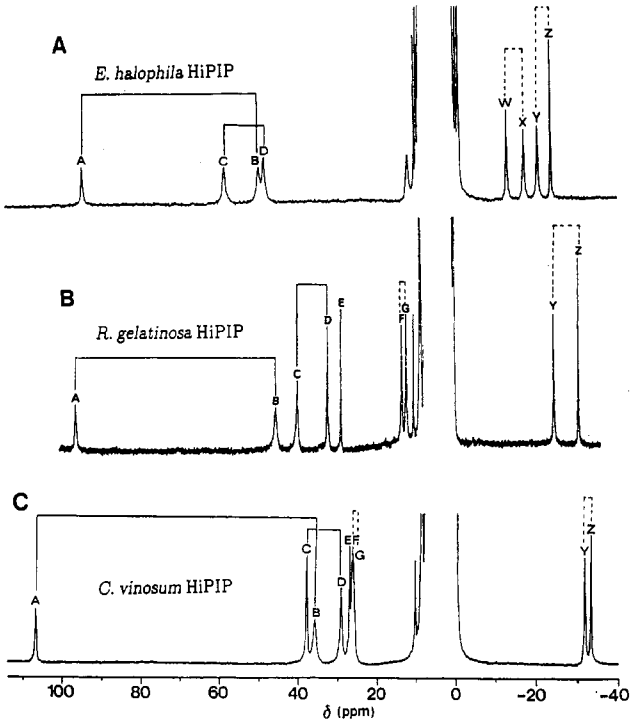

Figure 2. 298 K 600-MHz ^1H NMR spectra of D_2O solutions of oxidized HiPIPs from *E. halophila* (A, HiPIP II),[27] *R. gelatinosus* (B), and *C. vinosum* (C).[26] The samples are in 30 mM phosphate buffer at pH* 5.1. Note that in *C. vinosum* HiPIP at pH* = 7.0 and 298 K signals Y and Z are reversed.

For less symmetric coupling schemes the C_{im} coefficients can be obtained numerically.

Results

NMR Characterization of the Oxidized Form. The 600-MHz ^1H NMR spectrum of oxidized HiPIP from *R. gelatinosus* is reported in Figure 2B. For comparison purposes the spectra of oxidized HiPIP from *C. vinosum*[26] (Figure 2C) and *E. halophila*[27] (Figure 2A) are also shown. The signals in the latter two spectra are labeled in such a way to make them consistent with those of

Table I. 600-MHz ^1H NMR Shifts, T_1 Values, and NOE Connectivities at 300 K for the Isotropically Shifted Signals of the Oxidized HiPIP from *Rhodocyclus Gelatinosus*

signal	δ, ppm	T_1, ms[a]	irr signal	% NOE
A	95.8	8.4	B	6.0
B	45.1	6.6	A	6.3
C	39.6	9.7		
D	31.9	14.2	C	14.2
E	28.4	34.0	C	4.5
			D	4.6
F	13.0	8.5	G	7.5
G	11.9	10.9		
Y	−24.8	9.2		
Z	−30.9	25.4	Y	23.4

[a] Estimated by using the inversion recovery pulse sequence.[31] Estimated error ±20%.

R. gelatinosus (see Discussion). The NMR parameters of the isotropically shifted signals are reported in Table I. In the spectrum of *R. gelatinosus* seven isotropically shifted signals (A–G) are located in the 100/10 ppm region whereas two others (Y,Z) are in the −20/−40 ppm range. These signals are due to protons sensing the unpaired electrons on the metal ions and therefore belonging to residues directly coordinated to the metal ions. In Figure 3B the temperature dependence of the chemical shifts of the paramagnetically shifted signals A–G and Y,Z of *R. gelatinosus* are reported. For comparison purposes, also the temperature dependence of the other HiPIP's investigated by our laboratory are reported (Figure 3A,C).[26,27] As already observed in the HiPIP from *C. vinosum*, signals F,G follow an anti-Curie type behavior; i.e., they increase in shift with increasing temperature, although the slopes for the *C. vinosum* and *R. gelatinosus* proteins are different. It is interesting to note that signals A–D and Y,Z have similar behavior in the three proteins. The crossing observed between signals Y and Z in *C. vinosum* and *E. halophila* is likely to occur also in *R. gelatinosus* slightly outside the investigated temperature range. This crossing might be due to slight conformational changes on one methylene group with temperature, which superimposes to the temperature dependence of its two protons, and it is not further investigated here.

On the other hand, there is a set of two signals (F,G) that are slightly downfield in *R. gelatinosus*, more downfield in *C. vinosum*,

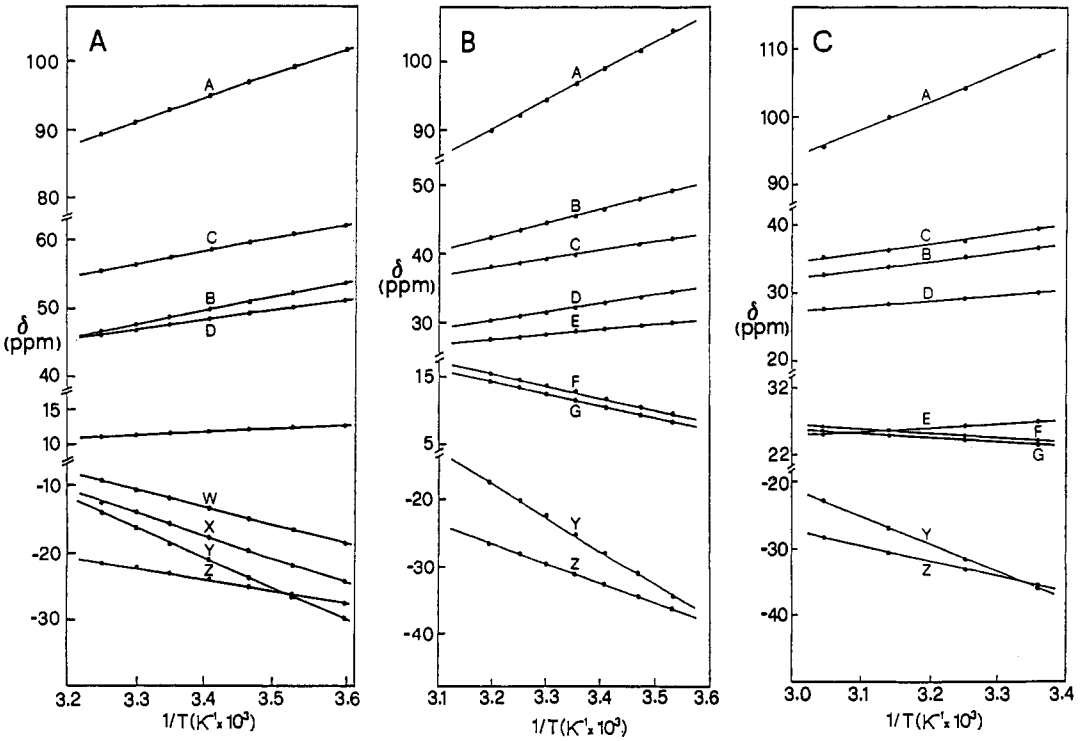

Figure 3. Temperature dependence of the chemical shifts of the hyperfine-shifted signals of oxidized HiPIPs from *E. halophila* (A)[27] and *R. gelatinosus* (B) at pH* = 5.1 and *C. vinosum* (C) at pH* = 7.0.[26]

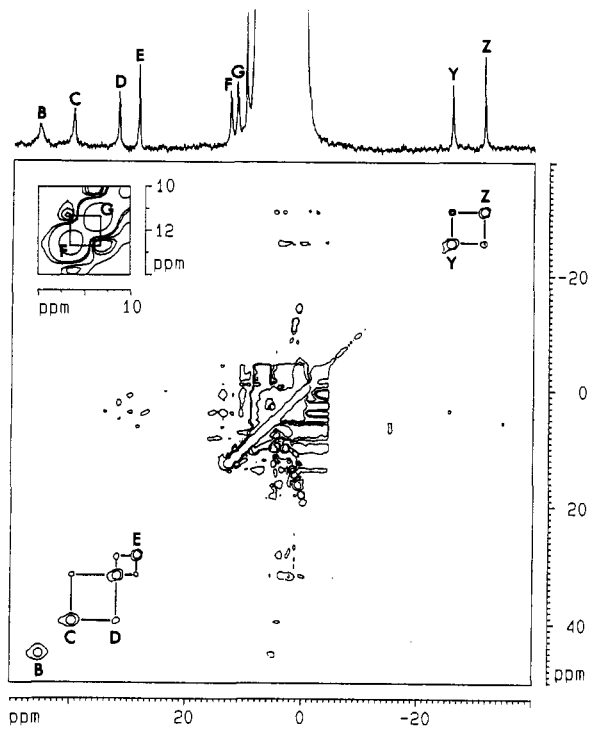

Figure 4. ^{1}H NOESY spectrum of D_2O solutions of oxidized HiPIP from *R. gelatinosus*. The sample is in 30 mM phosphate buffer at pH* 5.1 and 300 K. The acquisition and processing conditions are reported in the Experimental Section. The inset shows the F–G connectivity.

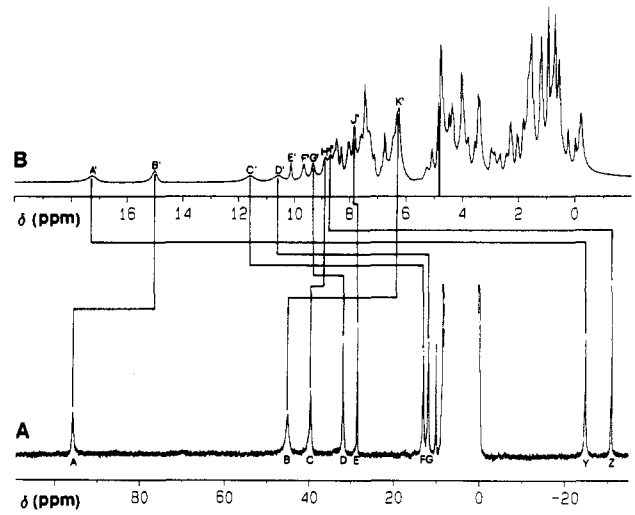

Figure 5. 298 K 600-MHz ^{1}H NMR spectra of the oxidized (A, pH* = 5.1, 30 mM phosphate buffer) and reduced (B, pH* = 7.0, 30 mM phosphate buffer) forms of *R. gelatinosus* HiPIP. The correspondences between signals in the two spectra are obtained through either EXSY or saturation-transfer experiments (see text).

and not observed in *E. halophila*, which, however, shows two more signals (W,X) in the upfield region. We have proposed[26,27] and we will further substantiate here that the signals W,X in *E. halophila* do correspond to the F,G pair in the other systems.

In order to assign the paramagnetically shifted signals, we have carried out ^{1}H nuclear Overhauser effect measurements, as already performed on the other investigated systems.[23,26,27] The NOESY spectrum in Figure 4 clearly shows the dipolar connectivities within three of the four β-CH_2 pairs and thus confirms the assignments of the signals C,D, F,G, and Y,Z to geminal β-CH_2 protons of the cysteine ligands; a dipolar connectivity is also apparent between the E and D signals. The dipolar connectivity between A and B, which is not apparent in the NOESY spectrum, has been confirmed by ^{1}H NOE experiments. The pairs of signals connected through NOE in the three proteins are summarized in Figure 2. In Table I the quantitative NOE values estimated from 1D experiments between the isotropically shifted signals are also reported. The strongest NOE's among the isotropically shifted signals are expected for geminal protons. The interproton distances evaluated by using the T_1 reported in Table I, and assuming a τ_c value of 3×10^{-9} s, are in the range 1.6–1.8 Å, thus confirming the assignments of signals A,B, C,D, F,G (or W,X), and Y,Z to geminal β-CH_2 protons of the cysteine ligands. This assignment is quite consistent with the present capabilities of the technique. The information is based on estimated distances. The detection of scalar connectivities would be a final proof of the assignment. We are working at extending the capabilities of NMR to detect COSY cross peaks between signals.

Proton E is close to one β-CH_2 proton of a cysteine (signal C), their distance being 2.3 Å. The temperature dependence of signal E is of Curie type and similar to that of signals C and D. This signal might be due to the corresponding α-CH, although further evidence is needed for a firm assignment.

NMR Characterization of the Reduced Form and Saturation Transfer. An EXSY experiment has been performed on 50% oxidized *R. gelatinosus* HiPIP. Cross peaks have been observed, indicating chemical exchange, between four signals of β-CH_2 of two cysteines of the oxidized form (C,D and Y,Z, Figure 5A) and the corresponding signals of the reduced species (H',G' and A',I', respectively, Figure 5B) and between signal E and its corresponding partner in the reduced form at 7.8 ppm (J'). Correlation between A and B (oxidized) with B' (15.0 ppm) and a broad signal at 6.2 ppm (K'), respectively, has been achieved by 1D saturation-transfer experiments. Also the correlation between signals F (13.2 ppm) and G (11.9 ppm), which are the β-CH_2 protons of one cysteine in the oxidized form, and signals C' (11.6 ppm) and D' (10.6 ppm) of the reduced form, respectively, has been obtained by 1D experiments. The correspondence between the signals of the oxidized and reduced forms is reported in Figure 4. From the assignment of the spectrum of the oxidized form and from the saturation-transfer experiments we can obtain the assignment of the NMR signals of the β-CH_2 cysteine protons in the reduced form. An NOE experiment has been also performed in the latter system on signals A' and B', which are well outside the diamagnetic envelope and well resolved. Clear NOE's on signals I' and K', respectively, were observed, as expected.

The spectra of reduced HiPIPs are similar to each other[26,27] and are similar to oxidized ferredoxins.[17] In particular, a close correspondence is observed between the oxidized–reduced form correlations in the present system (Figure 4) and in the *C. vinosum* protein.[26] The diamagnetic ground state and an anti-Curie behavior of all the isotropically shifted signals can be obtained under a number of combinations of J parameters. Among these, it would be tempting to say the two mixed-valence pairs with $S' = {}^9/_2$ are antiferromagnetically coupled.[17]

Discussion

We are going to show here that the present results give further evidence that the three HiPIP's have NMR spectra reconducible to a simple pattern. Although the spectral differences passing from *E. halophila* to *C. vinosum* through the presently studied *R. gelatinosus* are relatively large, there is a correspondence among the pairs of signals, as revealed by NOE measurements, in terms of shift values and their temperature dependence. Indeed, in the three proteins there are (1) one pair of signals downfield with a large chemical shift separation and Curie behavior (A,B), (2) one pair of signals downfield with a smaller chemical shift separation and Curie behavior (C,D), and (3) one pair of signals upfield with a small chemical shift separation and a pseudo-Curie behavior (Y,Z). The pseudo-Curie behavior is defined as a decrease in hyperfine shift with increasing temperature in the investigated temperature range, whose extrapolation at infinite temperature would lead to shifts of opposite sign.[26] It is very likely that all of these correspondences are not fortuitous but are due to a pattern related to the actual charges on the iron ions; i.e., it is likely that each pair of protons belongs to cysteine residues bound to a given type of iron. On the other hand, the fourth pair of signals is found upfield in *E. halophila* (W,X; pseudo-Curie), sizeably downfield

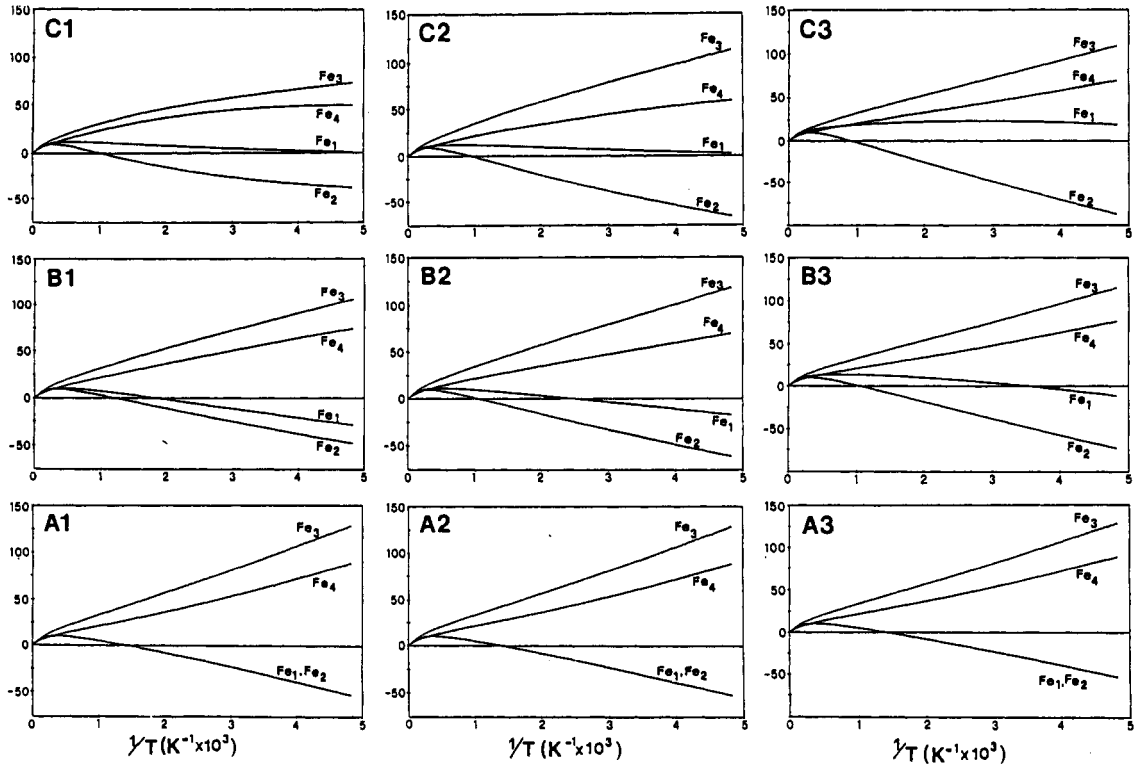

Figure 6. Calculated temperature dependences of the ^{1}H NMR hyperfine shifts of HiPIPs. Case 1: J_{12} = 400 cm^{-1}, J_{34} = 200 cm^{-1}, $J_{13} = J_{23} = J_{24}$ = 300 cm^{-1}, and J_{14} = 300 cm^{-1} (A1), 270 cm^{-1} (B1), and 230 cm^{-1} (C1). Case 2: J_{12} = 400 cm^{-1}, J_{34} = 200 cm^{-1}, $J_{23} = J_{24}$ = 300 cm^{-1}, and $J_{13} = J_{14}$ = 300 cm^{-1} (A2), 280 cm^{-1} (B2), and 270 cm^{-1} (C2). Case 3: J_{34} = 200 cm^{-1}, $J_{23} = J_{24}$ = 300 cm^{-1}, $J_{13} = J_{14} = 300 - x$ cm^{-1}, $J_{12} = 400 - x$ cm^{-1}, and x = 0 (A3), 30 (B3), and 50 cm^{-1} (C3). The calculations were performed numerically by using Hamiltonian (A1) (see Appendix). Cases A1 = A2 = A3 can also be computed by using the analytical solution of Hamiltonian (A2) (eq A3 and 6). Case C3 corresponds to halfway in the correlation diagram of Figure 7.

Chart I

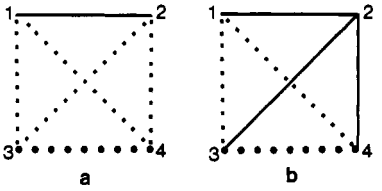

in *C. vinosum* (F,G; anti-Curie), and slightly downfield in *R. gelatinosa* (F,G; anti-Curie). We ascribe this behavior to differences in the electronic structure of the cluster in the three proteins. [A reviewer has suggested the possibility that the variability in chemical shift of the W,X/F,G pair and its temperature dependence be due to a conformational change rather than to an electronic effect. The most conceivable small change that can occur in a cluster of this type is a change in the dihedral angle Fe–S–C–H for the methylene protons. Such a change would tend to make the chemical shifts of the two signals either more or less equivalent, but would hardly account for an opposite temperature dependence of both or even a change in sign of the shift. On the contrary, a temperature dependence of conformation could be responsible for the behavior of the Y,Z pair.]

In order to better understand the behavior of the pair of signals F,G (or W,X) in the three proteins, we have performed a series of calculations as described in the Appendix and in the Materials and Methods section. In the starting situation Fe_1 and Fe_2 (see Figure 1) are taken to be pure iron(III) ions coupled with J_{12} = 400 cm^{-1} and Fe_3 and Fe_4 are taken to be the iron(III) and iron(II) ions of the mixed-valence pair, respectively, coupled with a constant J_{34} = 200 cm^{-1}. [This is the pair that will show electron delocalization upon introduction of the double-exchange term in the Hamiltonian (see later).] All the other coupling constants (J_{13}, J_{14}, J_{23}, J_{24}) are taken as 300 cm^{-1} (Chart Ia). Under these conditions Hamiltonian (A2) holds and energies given by eq A3 are obtained. The temperature dependence of the isotropic shifts, calculated according to eq 2 with the C_{im} values in eq 3, is reported in Figure 6A. In this situation two iron(III) ions (Fe_1, Fe_2) are equivalent and induce, on the protons sensing them, upfield shifts with pseudo-Curie behavior. The other iron(III) ion (Fe_3) induces downfield shifts, whereas those induced by iron(II) (Fe_4) are still downfield but smaller, both Fe_3 and Fe_4 having a Curie temperature dependence. The large J_{12} value between Fe^{3+} ions is consistent with their oxidation state. The smaller J value between Fe_3 and Fe_4 can be thought as being due to a decrease of the total antiferromagnetic contribution due to an implicit electron delocalization term[4,10] that brings about a ferromagnetic contribution. In other words, the small J_{34} value could be viewed as an antiferromagnetic coupling constant partially quenched by an explicit delocalization term. The energy levels given by eq A3 in this case would be further split by an extra term of the type $\pm B(S_{34} + {}^1/_2)$, where B is proportional to the electron delocalization. The shifts of iron(II) and iron(III) would be averaged equal if B is large enough, the actual difference being ascribed to the axial or equatorial nature of the methylene protons and to the asymmetry induced by the protein.[26] That is how we account for Fe_3 and Fe_4 being a mixed-valence pair.

Such a scheme was used as a crude approximation for the temperature behavior of the shifts of *C. vinosum*[26] but later shown to be more appropriate for *E. halophila*.[27] By keeping in mind that the actual value of J may be the result of different contributions including electron delocalization, we proceed by using simple Heisenberg Hamiltonians to a further analysis of the data.

Through eq A1 we can move from the situation in Figure 6A1 and decrease the symmetry by varying one or more coupling constants. For example, by decreasing J_{14}, i.e. by decreasing the coupling between one "pure" iron(III) (Fe_1) and the iron(II) of the mixed-valence pair (Fe_4), removal of the degeneracy between Fe_1 and Fe_2 (the two iron(III) ions not involved in the mixed-valence pair) is obtained (Figure 6B1). In general, by decreasing J_{14}, we observe a decrease of the shifts induced by all the iron ions, and for $J_{14} \leq 240$ cm^{-1} the shifts induced by Fe_1 result to be downfield at room temperature, passing from a pseudo-Curie to an anti-Curie behavior (Figure 6C1). This is the pattern

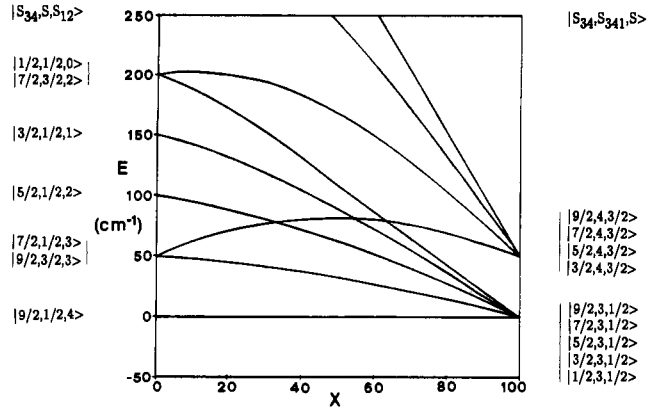

Figure 7. Low-lying energy levels for oxidized HiPIPs in the Heisenberg exchange-coupling scheme (Hamiltonian (A1)) calculated with $J_{23} = J_{24} = 300$ cm^{-1}, $J_{34} = 200$ cm^{-1}, $J_{12} = 400 - x$ cm^{-1}, $J_{13} = J_{14} = 300 - x$ cm^{-1}, and x varying from 0 to 100 cm^{-1}. The left-hand-side limit (Chart Ia) can be obtained from the analytical solution (eqs A3 and 6) of Hamiltonian (A2), while the right-hand-side limit (Chart Ib) can be obtained from the analytical solution (eqs A5 and 7) of Hamiltonian (A4).

observed for *R. gelatinosus* and *C. vinosum*. It should be noted that the shifts induced by Fe_3 and Fe_4 remain rather similar to one another from Figure 6A1 to 6C1, and therefore similar to their average, should electron delocalization within the Fe_3Fe_4 pair be introduced in the model. This is a general feature that is also encountered in all the subsequent cases.

A pattern similar to that of Figure 6A1–C1 can be reproduced by lowering J_{13} and J_{14} at the same time, but to a smaller extent (Figure 6A2–C2). Note that we are still involving Fe_1 in the change of magnetic coupling with Fe_3 and Fe_4. The experimental patterns can be reproduced by J_{14} and J_{13} in the ranges 280–270 cm^{-1} for *R. gelatinosus* and 270–260 cm^{-1} for *C. vinosum*.

It is apparent that the experimental data can be reproduced by any perturbation that makes Fe_1 and Fe_2 inequivalent and maintains J_{34} as the smallest of all J values.

Although the experimental data do not allow us to discriminate among the various combinations, more can be learned by showing a correlation diagram between the two limiting situations that can be described by analytical eqs A2 and A3 on the one hand and A4 and A5 on the other. In terms of Figure 1, we will pass from a situation in which Fe_1 and Fe_2 are equivalent and equally coupled to the Fe_3Fe_4 mixed-valence pair (Chart Ia) to another situation in which Fe_1, Fe_3, and Fe_4 are equally coupled and Fe_2 is coupled to the former three by a larger J (Chart Ib). This situation can be thought to arise, for example, by a weakening of the exchange interactions of Fe_1 with the other three metal ions. With this in mind we have allowed also J_{12}, in addition to J_{13} and J_{14} as in the case of Figure 6A2–C2, to decrease, in such a way to reach a symmetric case where $J_{23} = J_{24} = J_{12} = 300$ cm^{-1} and $J_{13} = J_{14} = J_{34} = 200$ cm^{-1}. This case, independently of how unrealistic it can be, is an interesting limit case in which Fe_1, Fe_3, and Fe_4 are equivalent, a situation that could correspond to a +2.66 charge on these three ions, where delocalization is allowed to be extended to a third iron center. The case of complete delocalization on a Fe_3S_4 center has been considered previously.[8,9] The other limiting case is that already discussed corresponding to the case of oxidized *E. halophila* HiPIP with the Fe_3–Fe_4 pair equivalent on one side and Fe_1–Fe_2 on the other. In this case delocalization would only be allowed to occur within the Fe_3–Fe_4 pair.

The lowest lying energy levels for the intermediate situations between the two limiting cases discussed above are reported in Figure 7. It appears that there is a smooth transition between the ground state formed by $S = {}^1/_2$, $S_{12} = 4$, and $S_{34} = {}^9/_2$ (left-hand side, *E. halophila* case) and that formed by $S = {}^1/_2$, $S_{134} = 3$, and $S_{34} = {}^9/_2$ (right-hand side). Only at the right-hand-side limit the ground state becomes degenerate with other states with $S = {}^1/_2$, $S_{134} = 3$, and $S_{34} = {}^1/_2, {}^3/_2, {}^5/_2$, and ${}^7/_2$. There is no crossing of the ground state with excited states. It appears therefore that the experimental pattern for *C. vinosum* and *R. gelatinosus* can be reproduced (see Figure 6A3–C3) by a situation that is approximately halfway in the correlation diagram of Figure 7.

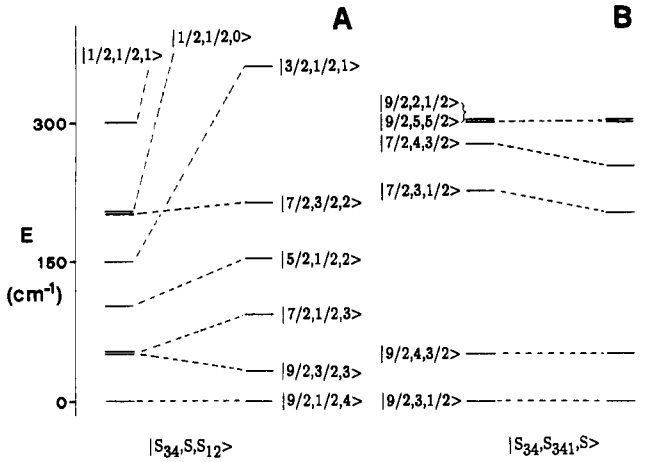

Figure 8. Effect of the introduction of the double-exchange parameter B on the low-lying energy levels of oxidized HiPIPs. The left-hand sides of the A and B diagrams are related to the left- and right-hand sides of Figure 7, respectively, as follows: A, $J_{13} = J_{14} = J_{23} = J_{24} = 300$ cm^{-1}, $J_{34} = 200$ cm^{-1}, and $J_{12} = 400$ cm^{-1}; B, $J_{12} = J_{23} = J_{24} = 300$ cm^{-1}, $J_{13} = J_{14} = 200$ cm^{-1}, and $J_{34} = 150$ cm^{-1}. The right-hand sides of the A and B diagrams are calculated by utilizing Hamiltonians (A6) and (A7), respectively, as follows: A, $J_{13} = J_{14} = J_{23} = J_{24} = J_{34} = 300$ cm^{-1}, $J_{12} = 390$ cm^{-1}, and $B_{34} = 390$ cm^{-1}; B, $J_{12} = J_{23} = J_{24} = 300$ cm^{-1}, $J_{13} = J_{14} = J_{34} = 200$ cm^{-1}, and $B_{34} = 200$ cm^{-1}.

The degeneracy of the various S_{34} values on the right-hand side of the diagram in Figure 7 suggests that we may also have $S_{12} = {}^7/_2$ and $S_{34} = 3$ as a ground state for *C. vinosum* and *R. gelatinosus*. Such a ground state may even be obtained for the limit situation at the left-hand side under a narrow choice of parameters. This does not change the general conclusions that by lowering of the symmetry the experimental pattern of the hyperfine coupling with the two iron(III) ions is reproduced.

The results of these calculations show that slight changes in the J parameters provide large variations on the hyperfine interaction values. This is due to a mechanism known as the *spin frustration mechanism*.[5] Such a mechanism forces for example one pair in a trinuclear cluster described by three antiferromagnetic J values to be "ferromagnetically" coupled if it experiences a smaller J value.[36] It has been shown that ferromagnetically coupled pairs have also a lower electron exchange barrier, and therefore, they may more easily show electron delocalization.[10]

We would like to show now that calculations including the double-exchange term (Hamiltonians (A6) and (A7)) give rise to the same ground state and similar pattern of lowest lying excited states, provided that J_{34} is properly changed. Figure 8 shows the close similarity in the lowest lying energy levels for the high-symmetry situations described by Hamiltonians (A2) and (A6) (Figure 8A) or (A4) and (A7) (Figure 8B). It is reasonable to believe that also in the low-symmetry intermediate case, pertinent to oxidized HiPIP from *C. vinosum* and *R. gelatinosus*, the description with Hamiltonian (A1) with only J's would be qualitatively similar to one with the B values. The covariance between B and J suggested by Figure 8 may also hold when more than one B is needed. The above considerations do not imply a preference on our side for a pure Heisenberg Hamiltonian model versus a model including a resonance term. We have applied the former because it is computationally simpler and still capable of mimicking the effect of a resonance term. Although a resonance term is undoubtedly present, its magnitude can only be obtained from a direct measurement and/or accurate fitting of extensive sets of experimental data (NMR, magnetic susceptibility, Mössbauer, ENDOR) of as high quality as those achieved on model compounds over a very large temperature range.[1,35,38,39]

(38) Rius, G.; Lamotte, B. *J. Am. Chem. Soc.* **1989**, *111*, 2464.

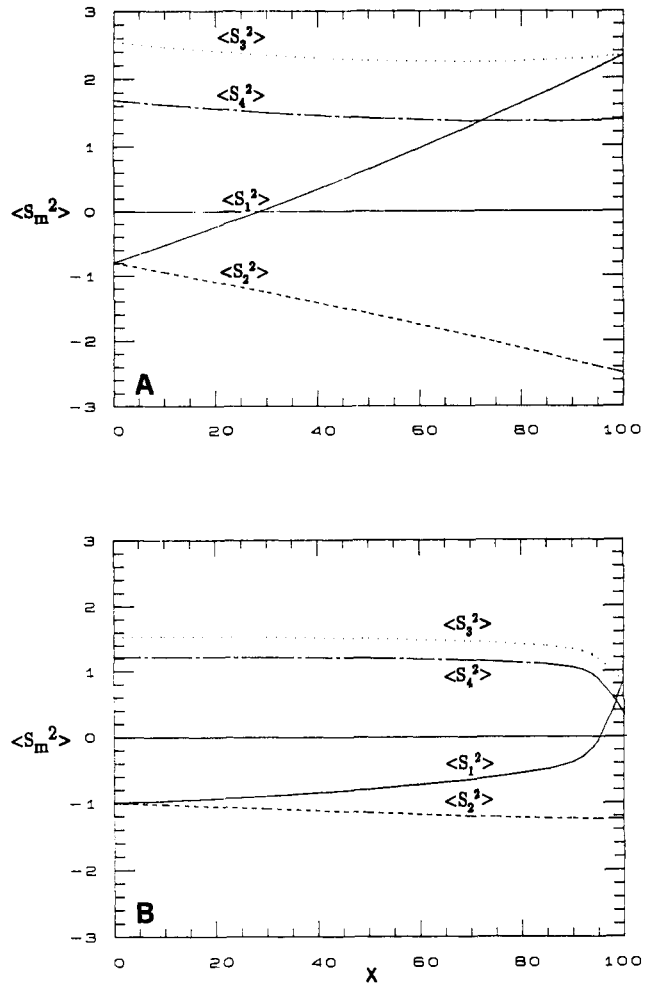

Figure 9. Correlation diagram showing the $\langle S_m^2 \rangle$ values (proportional to $-\langle S_{mz} \rangle$ in the low magnetic field limit) of each metal ion m under the same set of J values of Figure 6A3,B3,C3 at 300 K (A) and 4.2 K (B). $\langle S_1^2 \rangle$ becomes positive for $x > 30$ cm^{-1} at 300 K but only for $x > 90$ cm^{-1} at 4.2 K. The calculated values range between 3 and −3 at room temperature and between 2 and −2 at liquid-helium temperature. For ease of reference, in an uncoupled system $\langle S_m^2 \rangle = S_m(S_m + 1)$, i.e. $^{35}/_4$ for $S_m = {}^5/_2$ and 6 for $S_m = 2$.

Independently of the model, it is worth stressing that the picture coming out from the present considerations (Figure 7) is nicely consistent, besides the room-temperature NMR data on the three proteins, also with the liquid-helium Mössbauer data on the HiPIP from *C. vinosum*. The experimental data for the latter protein show that at room temperature the hyperfine interaction with one of the four metal ions is positive (upfield shifts in NMR), while at liquid-helium temperature two hyperfine interactions are positive. Figure 9 shows the variations of the $\langle S_m^2 \rangle$ values (proportional to $-\langle S_{mz} \rangle$ as long as $g_e \mu_B B_0 < kT$) for the four metal ions on passing from one limit situation (eqs A2 and A3) to the other (eqs A4 and A5) calculated at 300 K (A) and 4.2 K (B). At high temperature the $\langle S_1^2 \rangle$ value becomes positive (i.e. negative hyperfine interaction) rather soon, while at low temperature it stays negative until very close to the right-hand-side limit. Therefore, this picture accounts for the conclusion from Mössbauer data on *C. vinosum* that two iron(III) ions are indeed iron(III) and equal within the accuracy of the method, whereas NMR shows that the two iron(III) ions are quite inequivalent in oxidized HiPIP from *C. vinosum* and *R. gelatinosus*. The isotropic shift of one of the two iron(III) ions can thus be similar to those of the mixed-valence pair even without invoking the extension to the third iron(III) ion of the delocalization of the extra electron residing on the mixed-valence pair.

(39) Jordanov, J.; Roth, E. K. H.; Fries, P. H.; Noodleman, L. *Inorg. Chem.* **1990**, *29*, 4288.

The same results are obtained for the $S_{34} = {}^7/_2$ and $S_{12} = 3$ ground state. It should be noted that this case, although not discussed at length here because theoretically less probable and not proven by any experiment, could actually be in better agreement with the reported hyperfine coupling values from Mössbauer data.[28]

Appendix

In order to treat the more general cases, i.e. without any symmetry assumption, we describe the magnetic coupling among the four iron ions with the following spin Hamiltonian (Figure 1):

$$\hat{\mathcal{H}} = J_{12}\hat{\mathbf{S}}_1\cdot\hat{\mathbf{S}}_2 + J_{13}\hat{\mathbf{S}}_1\cdot\hat{\mathbf{S}}_3 + J_{14}\hat{\mathbf{S}}_1\cdot\hat{\mathbf{S}}_4 + J_{23}\hat{\mathbf{S}}_2\cdot\hat{\mathbf{S}}_3 + J_{24}\hat{\mathbf{S}}_2\cdot\hat{\mathbf{S}}_4 + J_{34}\hat{\mathbf{S}}_3\cdot\hat{\mathbf{S}}_4 \quad \text{(A1)}$$

Here $\hat{\mathbf{S}}_1$, $\hat{\mathbf{S}}_2$, $\hat{\mathbf{S}}_3$, and $\hat{\mathbf{S}}_4$ are the spin angular momentum operators of the different iron centers and the J_{mn} values are the two-center isotropic exchange-coupling constants. By operation with this spin Hamiltonian on the spin functions containing the isolated metal ion spin functions (of the type $|S_1,M_{S_1},S_2,M_{S_2},S_3,M_{S_3},S_4,M_{S_4}\rangle$) a matrix of 1080 × 1080 for the case of three iron(III) and one iron(II) is obtained, whose numerical diagonalization provides the eigenvalues and the eigenfunctions of all the spin states S_i' of the coupled system. [The matrix can be arranged in blocks, the largest block being 125 × 125. All calculations were performed in double precision.] In the case of only three different J coupling constant values, and under certain symmetry restrictions, analytical solutions are possible.[4,35] In order to proceed with the corresponding Hamiltonians, reference is necessary to Figure 1. Under the assumption that $J_{13} = J_{14} = J_{23} = J_{24} = J$, $J_{12} = J + \Delta J_{12}$, and $J_{34} = J + \Delta J_{34}$, Hamiltonian (A1) can be expressed as

$$\hat{\mathcal{H}} = J(\hat{\mathbf{S}}_1\cdot\hat{\mathbf{S}}_2 + \hat{\mathbf{S}}_1\cdot\hat{\mathbf{S}}_3 + \hat{\mathbf{S}}_1\cdot\hat{\mathbf{S}}_4 + \hat{\mathbf{S}}_2\cdot\hat{\mathbf{S}}_3 + \hat{\mathbf{S}}_2\cdot\hat{\mathbf{S}}_4 + \hat{\mathbf{S}}_3\cdot\hat{\mathbf{S}}_4) + \Delta J_{12}(\hat{\mathbf{S}}_1\cdot\hat{\mathbf{S}}_2) + \Delta J_{34}(\hat{\mathbf{S}}_3\cdot\hat{\mathbf{S}}_4) \quad \text{(A2)}$$

where J is the iron–iron isotropic exchange-coupling constant and ΔJ_{12} and ΔJ_{34} are the deviations from J of the exchange-coupling constants between the iron centers in the 1–2 and 3–4 pairs (referenced to the labeling of Figure 1). The corresponding expression for the energies of the spin levels in the cluster is[4,26]

$$E(S_{12}S_{34}S) = (J/2)[S(S+1)] + (\Delta J_{12}/2)[S_{12}(S_{12}+1)] + (\Delta J_{34}/2)[S_{34}(S_{34}+1)] \quad \text{(A3)}$$

where $|S_{12} + S_{34}| \geq S \geq |S_{12} - S_{34}|$, $|S_1 + S_2| \geq S_{12} \geq |S_1 - S_2|$, and $|S_3 + S_4| \geq S_{34} \geq |S_3 - S_4|$.

In the case of $J_{12} = J_{23} = J_{24} = J$, $J_{13} = J_{14} = J + \Delta J_{341}$, and $J_{34} = J + \Delta J_{341} + \Delta J_{34}$, the Hamiltonian (A1) takes the form

$$\hat{\mathcal{H}} = J(\hat{\mathbf{S}}_1\cdot\hat{\mathbf{S}}_2 + \hat{\mathbf{S}}_1\cdot\hat{\mathbf{S}}_3 + \hat{\mathbf{S}}_1\cdot\hat{\mathbf{S}}_4 + \hat{\mathbf{S}}_2\cdot\hat{\mathbf{S}}_3 + \hat{\mathbf{S}}_2\cdot\hat{\mathbf{S}}_4 + \hat{\mathbf{S}}_3\cdot\hat{\mathbf{S}}_4) + \Delta J_{341}(\hat{\mathbf{S}}_1\cdot\hat{\mathbf{S}}_3 + \hat{\mathbf{S}}_1\cdot\hat{\mathbf{S}}_4 + \hat{\mathbf{S}}_3\cdot\hat{\mathbf{S}}_4) + \Delta J_{34}(\hat{\mathbf{S}}_3\cdot\hat{\mathbf{S}}_4) \quad \text{(A4)}$$

where ΔJ_{341} is the deviation from J of the exchange-coupling constants between the iron centers in the 1–3, 1–4, and 3–4 pairs (refer to the labeling of Figure 1) and ΔJ_{34} is the further deviation of J_{34} from the other two. This picture requires Fe_2 to be equally antiferromagnetically coupled to the other three iron ions. Also in this case, analytical solutions can be obtained. The energies of the levels are

$$E(S_{34}S_{341}S) = (J/2)S(S+1) + (\Delta J_{341}/2)[S_{341}(S_{341}+1) - S_{34}(S_{34}+1)] + (\Delta J_{34}/2)S_{34}(S_{34}+1) \quad \text{(A5)}$$

where $|S_{341} + S_2| > S \geq |S_{341} - S_2|$, $|S_{34} + S_1| \geq S_{341} \geq |S_{34} - S_1|$, and $|S_3 + S_4| \geq S_{34} \geq |S_3 - S_4|$.

Note that in the former case four J values must be equal and the other two can differ from the former four as well as one from the other (Chart Ia), whereas in the latter case three J values must be equal, two other J values must be equal but can be different from the former, and the last value can differ from all the others (Chart Ib). For the former case, Hamiltonian (A2), we have chosen the situation in which, referring to Figure 1 and Chart Ia, J_{13}, J_{14}, J_{23}, and J_{24} are equal and J_{12} and J_{34} are different from the former and differ one from the other. For the latter case, Hamiltonian (A4), we have chosen the situation in which, referring to Figure 1 and Chart Ib, J_{12}, J_{23}, and J_{24} are equal, J_{13} and J_{14}

are equal, and J_{34} may or may not differ from J_{13} and J_{14}.

In an alternative to the simple Heisenberg description of the magnetic coupling within the cluster, expressed by Hamiltonians (A1), (A2), or (A4), a description that takes into account electron delocalization may be used. Such treatment is available for dinuclear species,[10] for the $[Fe_3S_4]^{0}$ [6-8] clusters, and for the $[Fe_4S_4]^{+}$ [9] and $[Fe_4S_4]^{3+}$ [4,26] clusters. In the case of the $[Fe_3S_4]^{0}$ clusters, it has been demonstrated that a simple Heisenberg treatment is capable of providing the same electronic description[36] as the model including electron delocalization.[5,6] This happens because there is large covariance between J values and the electron delocalization or, as generally called, the double-exchange parameter.[10] In the following, a B parameter that takes into account the tendency of the electrons to delocalize between ions at different oxidation states will be introduced according to a model previously proposed[4] and already used by us for describing the *C. vinosum* HiPIP.[26] In the presence of double exchange, Hamiltonians (A2) and (A4) are respectively transformed as[6,10]

$$\hat{\mathcal{H}} = [J(\hat{S}_1\cdot\hat{S}_2 + \hat{S}_1\cdot{}^3\hat{S}_3 + \hat{S}_1\cdot{}^3\hat{S}_4 + \hat{S}_2\cdot{}^3\hat{S}_3 + \hat{S}_2\cdot{}^3\hat{S}_4 + {}^3\hat{S}_3\cdot{}^3\hat{S}_4) + \Delta J_{12}(\hat{S}_1\cdot\hat{S}_2) + \Delta J_{34}({}^3\hat{S}_3\cdot{}^3\hat{S}_4)]\hat{O}_3 + [J(\hat{S}_1\cdot\hat{S}_2 + \hat{S}_1\cdot{}^4\hat{S}_3 + \hat{S}_1\cdot{}^4\hat{S}_4 + \hat{S}_2\cdot{}^4\hat{S}_3 + \hat{S}_2\cdot{}^4\hat{S}_4 + {}^4\hat{S}_3\cdot{}^4\hat{S}_4) + \Delta J_{12}(\hat{S}_1\cdot\hat{S}_2) + \Delta J_{34}({}^4\hat{S}_3\cdot{}^4\hat{S}_4)]\hat{O}_4 + B_{34}\hat{V}_{34}\hat{T}_{34} \quad (A6)$$

and

$$\hat{\mathcal{H}} = [J(\hat{S}_1\cdot\hat{S}_2 + \hat{S}_1\cdot{}^3\hat{S}_3 + \hat{S}_1\cdot{}^3\hat{S}_4 + \hat{S}_2\cdot{}^3\hat{S}_3 + \hat{S}_2\cdot{}^3\hat{S}_4 + {}^3\hat{S}_3\cdot{}^3\hat{S}_4) + \Delta J_{341}(\hat{S}_1\cdot{}^3\hat{S}_3 + \hat{S}_1\cdot{}^3\hat{S}_4 + {}^3\hat{S}_3\cdot{}^3\hat{S}_4) + \Delta J_{34}({}^3\hat{S}_3\cdot{}^3\hat{S}_4)]\hat{O}_3 + [J(\hat{S}_1\cdot\hat{S}_2 + \hat{S}_1\cdot{}^4\hat{S}_3 + \hat{S}_1\cdot{}^4\hat{S}_4 + \hat{S}_2\cdot{}^4\hat{S}_3 + \hat{S}_2\cdot{}^4\hat{S}_4 + {}^4\hat{S}_3\cdot{}^4\hat{S}_4) + \Delta J_{341}(\hat{S}_1\cdot{}^4\hat{S}_3 + \hat{S}_1\cdot{}^4\hat{S}_4 + {}^4\hat{S}_3\cdot{}^4\hat{S}_4) + \Delta J_{34}({}^4\hat{S}_3\cdot{}^4\hat{S}_4)]\hat{O}_4 + B_{34}\hat{V}_{34}\hat{T}_{34} \quad (A7)$$

where $\hat{O}_3$ and $\hat{O}_4$ are the occupation operators for sites 3 and 4, respectively,[6] $\hat{T}_{34}$ is the transfer operator between sites 3 and 4, and ${}^j\hat{S}_i$ (i = 3, 4; j = 3, 4) values represent the spin angular momentum operator $\hat{S}_i$ when the extra electron is on site j. B_{34} is a scalar factor proportional to the effectiveness of exchange, and $\hat{V}_{34}$ is an operator producing as eigenvalues $(S_{34} + {}^1/_2)$.[6] Such terms give the additional contributions to the energies in (A3) and (A5)

$$\pm B_{34}(S_{34} + {}^1/_2) \quad (A8)$$

In principle more than one B parameter could be used, but a report is available only for the Fe_3S_4 cluster.[8] The same order of the low-lying energy levels is obtained with and without B provided that at least one J value (the one that couples the spins connected by the transfer operator $\hat{T}_{ij}$) is properly changed. In the absence of independent information on B, the approach based only on J values is substantially equivalent to that including B.

Contribution from the Department of Medicinal Chemistry, School of Medicine, Hiroshima University, Kasumi, Minami-ku, Hiroshima 734, Japan, Coordination Chemistry Laboratories, Institute for Molecular Science, Myodaiji, Okazaki 444, Japan, and Shionogi Research Laboratories, Shionogi & Company Ltd., Fukushima-ku, Osaka 553, Japan

Synthesis, Properties, and Complexation of a New Imidazole-Pendant Macrocyclic 12-Membered Triamine Ligand

Eiichi Kimura,*[†,‡] Yasuhisa Kurogi,[†,‡] Mitsuhiko Shionoya,[†,‡] and Motoo Shiro[§]

Received May 15, 1991

A new 12-membered macrocyclic triamine with an imidazole-pendant group, 2-(4-imidazoyl)-1,5,9-triazacyclododecane (**5**), has been synthesized to study its complexation behavior with Zn^{II} and Cu^{II}, along with the ease with which the metal-bound imidazolate anion is generated. The Zn^{II} complex (**6a**) shows a close equatorial coordination of the imidazole (2.025 Å) in a distorted trigonal-bipyramidal structure with an additional chloride ion. Final R and R_w were 0.030 and 0.040, respectively: $C_{12}H_{23}N_5ZnCl(ClO_4)$, orthorhombic, space group $Pna2_1$, with a = 14.574 (1) Å, b = 9.079 (1) Å, c = 13.506 (1) Å, ρ_c = 1.627 (g cm^{-3}) for Z = 4, V = 1787.0 (3) Å^3. The proton dissociation most likely from the Zn^{II}- and Cu^{II}-coordinated imidazole (**6**, **7**) occurs with pK_a values of 10.3 and 9.3, respectively, at 25 °C and I = 0.1 (KNO_3). Mixtures of the Cu^{II} (or Zn^{II}) complex **6** and Cu^{II} (or Zn^{II}) [12]aneN$_3$ ([12]aneN$_3$ = 1,5,9-triazacyclododecane) complex **1** in alkaline CH_3OH solution yield Cu^{II},Cu^{II} (or Zn^{II},Zn^{II}) dinuclear complexes bridged by the imidazolate anion, **8**. A boron complex (**9**) has been isolated during the diborane reduction of the monooxo precursor **11**.

Introduction

Imidazole is one of the most common biofunctional ligands to play critical roles in hydrolytic nonmetallic enzymes (often "serine" enzymes) and metalloenzymes.[1] In carbonic anhydrase (CA), the Zn^{II}-bound imidazolate anion was once proposed to account for the catalytic mechanism, in which the observed proton dissociation with a pK_a value of ~7 was assigned to the imidazole (ImH) ⇌ imidazolate (Im^-) equilibrium ("zinc–imidazole" mechanism) as a result of the coordinating Zn^{II}.[2] However, the circumstantial evidence now overwhelmingly points to the H_2O ⇌ OH^- equilibrium ("zinc–hydroxide" mechanism).[3] Meanwhile, an extraneous imidazole inhibitor may replace the fourth coordinating H_2O site as an anionic Im^- ligand bonding to Zn^{II} at alkaline pH in CA.[4]

Until now, very few chemical models had been designed to test the effect of the metal coordination on ImH ⇌ Im^-. In 1976, Sargeson et al. prepared $[(NH_3)_5Co^{III}(ImH)]^{3+}$, where the $Co^{III}(ImH)$ ⇌ $Co^{III}(Im^-)$ equilibrium occurred with pK_a value of 10.0.[5] Thus, $Co^{III}(Im^-)$ had ca. 15 times higher nucleophilicity

Scheme I. Model for the CA Active Center

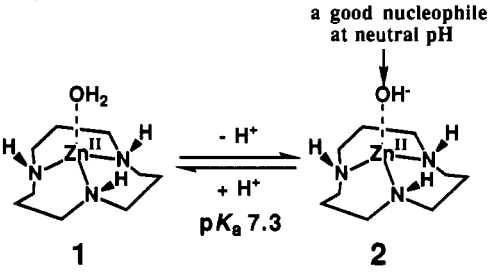

(1) Sundberg, R. J.; Martin, R. B. *Chem. Rev.* **1974**, *74*, 471.
(2) Pesando, J. M. *Biochemistry* **1975**, *14*, 675, 681.
(3) Buckingham, D. A. In *Biological Aspects of Inorganic Chemistry*; Addison, A. W., Cullen, W. R., Dolphin, D., James, B. R., Eds.; John Wily & Sons: New York, 1977; Chapter 5. Lindskog, S. In *Zinc Enzymes*; Bertini, I., Luchinat, C., Maret, W., Zeppezauer, M., Eds.; Birkhäuser: Boston, MA, 1986; Chapter 22.

[†] Hiroshima University.
[‡] Institute for Molecular Science.
[§] Shionogi and Co. Ltd.

0020-1669/91/1330-4524$02.50/0